

# Hard-disk dipoles and non-reversible Markov chains

Philipp Höllmer,<sup>1, a)</sup> A. C. Maggs,<sup>2, b)</sup> and Werner Krauth<sup>3, c)</sup>

<sup>1)</sup>*Bethe Center for Theoretical Physics, University of Bonn, Nussallee 12, 53115 Bonn, Germany*

<sup>2)</sup>*CNRS UMR7083, ESPCI Paris, Université PSL, 10 rue Vauquelin, 75005 Paris, France*

<sup>3)</sup>*Laboratoire de Physique de l'École normale supérieure, ENS, Université PSL, CNRS, Sorbonne Université, Université de Paris, Paris, France*

(Dated: 24 November 2021)

We benchmark event-chain Monte Carlo (ECMC) algorithms for tethered hard-disk dipoles in two dimensions in view of application of ECMC to water models in molecular simulation. We characterize the rotation dynamics of dipoles through the integrated autocorrelation times of the polarization. The non-reversible straight, reflective, forward, and Newtonian ECMC algorithms are all event-driven, and they differ only in their update rules at event times. They realize considerable speedups with respect to the local reversible Metropolis algorithm. We also find significant speed differences among the ECMC variants. Newtonian ECMC appears particularly well-suited for overcoming the dynamical arrest that has plagued straight ECMC for three-dimensional dipolar models with Coulomb interactions.

## I. INTRODUCTION

Markov-chain Monte Carlo<sup>1</sup> (MCMC) is a computational method for sampling high-dimensional probability distributions  $\pi$  including the Boltzmann distribution of statistical physics. In MCMC, an initial sample  $x$ , at a time  $t = 0$ , is drawn from a distribution  $\pi^{\{0\}}$  rather than from the “equilibrium” distribution  $\pi$ . The sample  $x$ , at time  $t$ , moves to the sample  $y$ , at time  $t + 1$ , with a conditional probability  $P_{xy}$ , element of a time-independent transition matrix  $P$ . The probability distribution  $\pi^{\{t\}}$  then moves to  $\pi^{\{t+1\}} = \pi^{\{t\}}P$ . The intermediate probability distributions are usually not known explicitly, but they evolve towards  $\pi$  for  $t \rightarrow \infty$ . The transition matrix  $P$  must satisfy a balance condition that expresses the stationarity of  $\pi$ . Reversible transition matrices satisfy the detailed-balance condition  $\pi_x P_{xy} = \pi_y P_{yx}$  for all  $x$  and  $y$ . Detailed balance is equivalent to the statement that the equilibrium flow  $\mathcal{F}_{xy} = \pi_x P_{xy}$  from  $x$  to  $y$  equals the reverse flow from  $y$  to  $x$ . Non-reversible MCMC algorithms satisfy a weaker global-balance condition  $\pi_x = \sum_y \pi_y P_{yx}$  for all  $x$ . Under conditions of irreducibility and aperiodicity,<sup>2</sup> they converge to the equilibrium distribution  $\pi$  with non-zero net flows  $\mathcal{F}_{xy} - \mathcal{F}_{yx}$ . Samples are then drawn from the equilibrium distribution  $\pi$  for  $t \rightarrow \infty$  by a non-equilibrium random process with non-vanishing net flows.

In past decades, research and applications have focused almost exclusively on reversible Markov chains (and some close relatives, such as sequential schemes<sup>3,4</sup>). Reversible Markov chains are straightforward to set up for arbitrary probability distributions  $\pi$ , and are easy to conceptualize, in particular because of the real-valued eigenvalue

spectrum of their transition matrices. Popular reversible Markov chains include the Metropolis<sup>1</sup> or heat-bath<sup>5–7</sup> algorithms. Interest in non-reversible Markov chains has increased in recent years, ever since it was understood<sup>8,9</sup> that such algorithms often approach equilibrium faster than reversible Markov chains. Systematic non-reversible Markov-chain schemes are becoming available.<sup>10,11</sup>

Event-chain Monte Carlo<sup>11–13</sup> (ECMC) is a family of non-reversible local Markov chains that have been applied to, e.g., particle<sup>14</sup> and spin systems,<sup>15–17</sup> polymers<sup>18,19</sup> and field-theoretical models.<sup>20</sup> ECMC algorithms are defined in continuous time, and they can be interpreted as piecewise deterministic Markov processes.<sup>21</sup> They have found applications in Bayesian statistics.<sup>22,23</sup> A number of features set ECMC algorithms apart from reversible Markov chains. First, they may reach the “equilibrium” distribution  $\pi$  on fast ballistic time scales rather than on the diffusive time scales that are typically associated with local reversibility. Considerable speedups were demonstrated in analytically solvable test cases<sup>8,9,24</sup> and recovered in applications of practical relevance.<sup>13,14,19,20</sup> Second, ECMC, for a given model (probability distribution  $\pi$ ), covers closely related local MCMC algorithms that can behave quite differently. Algorithms adopt a wide range of factor sets for the breakup of the Boltzmann distribution. On a finer scale, even for a given set of factors, different variants may have widely different behaviors, as we will discuss in the present paper. Third, ECMC need not evaluate the ratio  $\pi_y/\pi_x$  to move from a sample  $x$  to a sample  $y$  (in other words, need not evaluate the change in energy), because the factors are statistically independent.<sup>12,25</sup>

The sampling of the Boltzmann distribution without evaluating the energy is implemented in a general-purpose open-source ECMC application<sup>26</sup> for classical molecular simulation in Coulomb systems, where the evaluation of the energy represents for other methods the computational bottleneck. In the test case of three-dimensional water with the simple-point-charge-flexible-

<sup>a)</sup>Electronic mail: hoellmer@physik.uni-bonn.de

<sup>b)</sup>Electronic mail: anthony.maggs@espci.fr

<sup>c)</sup>Electronic mail: werner.krauth@ens.fr

water (SPC/Fw) potential<sup>27</sup> and the “periodic” variant of straight ECMC (see Section III B for a definition), the simulated water molecules however resisted rotation and the polarization remained dynamically arrested for long times.<sup>28</sup> The present paper studies many variants of ECMC for a simpler model of polar molecules, and suggests that its periodic variant is ill-suited to these systems.

In a generic Markov chain, the sample space  $\Omega$  is distinct from the moves  $\Delta$ . The latter are then part of a move set and lead from samples  $x \in \Omega$  to samples  $y \in \Omega$ . In the local reversible Metropolis algorithm for particle systems, for example,  $\Delta = (\delta, i)$  consists in a small random displacement  $\delta$  of a random particle  $i$ . ECMC, in contrast, belongs to the class of lifted Markov chains,<sup>8,9</sup> in which parts of the move set are integrated into a “lifted” sample space. In the above example, the proposed move  $\Delta' = (\delta', i')$  at time  $t + 1$ , after a move  $\Delta$ , at time  $t$ , is then no longer independently sampled, but it rather depends on the lifted configuration, and in particular on  $\Delta$ . The probability distribution lives itself in an extended space. Nevertheless, in the cases that we consider here, the stationary probability distribution in the lifted space factorizes into the original distribution  $\pi$  and a distribution for the lifting variables, while the transition matrix non-trivially couples the two sectors.

In this paper we caricature the SPC/Fw water model as tethered hard-disk dipoles. This replaces a three-dimensional model by a two-dimensional one, and lumps the vibrational, bending, Lennard-Jones, and Coulomb interactions into a hard-disk potential. The simplified dipole model retains the polar nature of molecules, and it can be simulated orders of magnitude faster than the system of flexible Coulomb dipoles. It also greatly simplifies the implementation of the different algorithms. This allows us to scan straight,<sup>11,29</sup> reflective,<sup>11</sup> forward,<sup>30</sup> and Newtonian<sup>31</sup> ECMC with thousands of parameter sets. We benchmark the ECMC algorithms against the local Metropolis algorithms with different displacement sets. We characterize the speed of algorithms *via* the autocorrelation of the polarization, the mode that with ECMC equilibrates slowly in the SPC/Fw water model.<sup>28</sup>

For dipole-model parameters that roughly correspond to those of SPC/Fw water, we find a 50-fold speedup for the fastest non-reversible ECMC algorithm with respect to the optimized local reversible Metropolis algorithm. We also find a more than order-of-magnitude speed difference among the different ECMC variants. The different versions of straight ECMC are clearly the slowest ones at low density, while they are comparable with forward and reflective ECMC at high densities. Newtonian ECMC is by far the fastest. We suggest that this is due to its absence of intrinsic parameters.

The content of this paper is as follows: In Section II, we define the two-dimensional tethered hard-disk dipole model and motivate its parameters with respect to physical systems of the SPC/Fw model in three dimensions. We also discuss the polarization, which tracks the abil-

ity of dipoles to rotate. In Section III, we discuss the reversible and non-reversible MCMC algorithms that we have implemented and illustrate their behavior for the case of a single dipole. We also discuss subtle aspects concerning the irreducibility of the Markov chains. In Section IV, we benchmark the different variants of ECMC against the local reversible Metropolis algorithm for a range of densities and system sizes, and we evidence the superiority of the non-reversible ECMC algorithms. In Section V, we project how our conclusions can be extended to the more complex water models.

## II. HARD-DISK DIPOLE MODEL

We consider tethered dipoles in a two-dimensional square box of sides  $L$  with periodic boundary conditions. Each dipole consists of two hard disks of radius  $\sigma$ , with a flat inner-dipole interaction that constrains its extension  $\rho$  (the separation of the disk centers) between the contact distance  $r = 2\sigma$  and the tether length  $R$  (see Fig. 1a). Dipole configurations without overlapping disks and with all dipole extensions between  $r$  and  $R$  all have the same Boltzmann weight, whereas all other configurations have zero statistical weight. As the minimum dipole extension at contact equals  $2\sigma$  (see Fig. 1a), each dipole configuration is also a configuration of hard disks. Any dipole system is parameterized by the number of dipoles  $N$ , the tether ratio  $\eta = R/r$ , and the hard-disk density  $D = 2N\pi\sigma^2/L^2$ .

In a single three-dimensional water molecule at room temperature (as for example described in the SPC/Fw model), the oxygen–hydrogen distance fluctuates by  $\sim 2.3\%$  and the hydrogen–hydrogen distance by  $\sim 3.4\%$  (see Fig. 1b). In the hard-disk dipole model, we thus adopt a tether ratio  $\eta = 1.1$ , for which the  $\sim 2.75\%$  fluctuations of the extension are quite similar. The tether length  $R$  is thus only 10% larger than the contact distance between two disks, so that two dipoles cannot lock into a crossed state that would be difficult to disentangle in two dimensions. Our results for the dynamics of two-dimensional models may well extend to three dimensions.

We measure dynamical information through the integrated autocorrelation functions of components of the total polarization  $\mathbf{p}$ :

$$\mathbf{p} = \sum_{i=1}^N \mathbf{p}_i, \quad (1)$$

where  $\mathbf{p}_i$  is the oriented separation vector between the two disks in the  $i$ th dipole, possibly corrected for periodic boundary conditions (see Fig. 1c and d).

For  $N = 1$ , analytic results are available for the dynamics of some of the algorithms discussed here.<sup>29</sup> The center-of-mass motion of the single dipole then factors out, and the sample space  $\Omega$  simply corresponds to the possible values of the polarization vector, in other words to the two-dimensional ring with inner radius  $r$  and outer

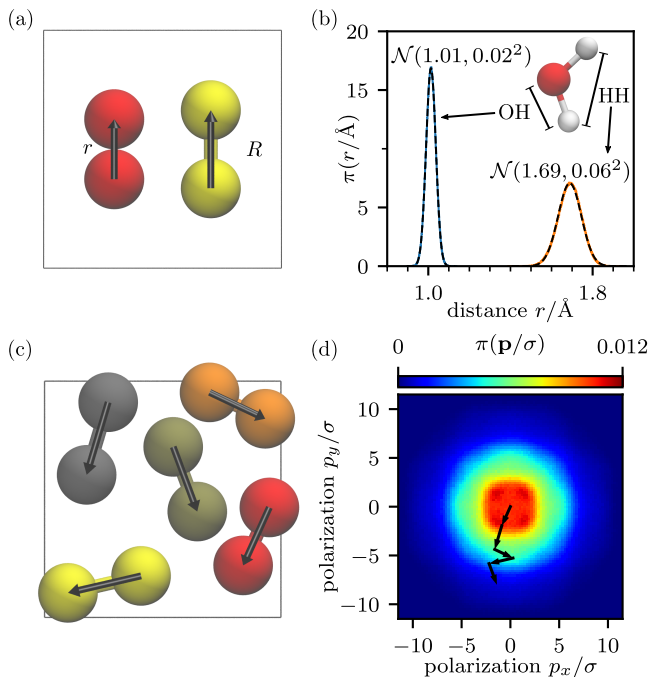


FIG. 1. Tethered hard-disk dipole model. (a): Dipoles with two hard disks of radius  $\sigma$ , and minimum extension  $r = 2\sigma$  and tether length  $R$ . (b): Probability distribution of the oxygen–hydrogen (OH) and hydrogen–hydrogen (HH) bond lengths for a single SPC/Fw water molecule at room temperature. (c): Five dipoles with polarization  $\mathbf{p}_i$ . (d): Total polarization  $\mathbf{p}$  of (c), together with its probability distribution.

radius  $R$  (see Ref. 29). The single-dipole polarization  $\mathbf{p}$  is uniformly distributed in this ring.

### III. REVERSIBLE AND NON-REVERSIBLE MCMC

In the present section, we introduce MCMC algorithms that will be used in Section IV. We also illustrate them for a single dipole ( $N = 1$ ) and review some of their fundamental properties. We only consider algorithms where at each moment a single disk moves, as this can also be realized within ECMC in the presence of long-range Coulomb interactions.<sup>25,26</sup> Dipole rotations—that relax the polarization—are thus pieced together from subsequent displacements of single disks. This has already proven efficient in ECMC for polymer models and for elongated hard needles.<sup>18,19</sup> Explicit dipole rotations appear difficult to put into place in this context.

The local MCMC moves discussed here feature small single-disk displacements at each time step (for the Metropolis algorithm) or continuous moves in time (for the ECMC algorithms). Again, this is motivated by the future applications to more complicated systems such as water, for which non-local moves including cluster updates<sup>32,33</sup> appear out of reach. Although we thus restrict our attention to a subclass of MCMC algorithms with

very similar design principles, we will show in Section IV that their properties differ substantially.

In the ECMC algorithms, a single active disk moves with a constant velocity in a given direction. The straight-line trajectories stop at events which correspond to hard-disk collisions or to the moment when the dipole extension reaches the tether length. In addition, resamplings take place at predefined MCMC times, which are separated by a chain time  $\tau_{\text{chain}}$ . Resamplings also interrupt the straight-line trajectory, and for example draw a new velocity and a new active disk.

#### A. Reversible local Metropolis algorithms

The local Metropolis algorithm,<sup>1</sup> for the dipole model, selects a random disk  $i$  at each time step. For the cross-shaped displacement set, the proposed move for  $i$  is sampled uniformly between  $-\delta$  and  $\delta$  with range  $\delta$ , randomly in  $x$ - or in  $y$ -direction. For the square-shaped displacement set, the proposed move is uniformly sampled from a square of sides  $2\delta$  centered at zero, with both the  $x$  and the  $y$  components of the displacement sampled independently between  $-\delta$  and  $\delta$ . In both cases, the move is accepted if it violates no constraints. If the move is rejected, the configurations at times  $t$  and  $t + 1$  are the same. The Metropolis algorithm, with the given displacement sets, satisfies the detailed-balance condition. For  $N = 1$ , the polarization  $\mathbf{p}$  performs a random walk in the sample space  $\Omega$ . The algorithm can be considered irreducible for all  $N$ , though some blocked configurations<sup>34</sup> may pose problems.<sup>35</sup>

#### B. Straight ECMC

In straight ECMC,<sup>11</sup> the velocity is of constant absolute value, and it changes only at resamplings. We analyze several variants for updating the angle  $\phi$  that describes the velocity in two dimensions. In the “periodic” variant, the angle alternates between  $\phi = 0$  and  $\phi = \pi/2$ . In arbitrary dimension, the velocity cycles through the unit vectors aligned with the positive coordinate axes. The periodic variant, used in most previous works, is implemented in the general-purpose ECMC application.<sup>26</sup> In the present paper, we also analyze the “random” variant where  $\phi$  is uniformly sampled in the interval  $[0, 2\pi)$  and, finally, the “sequential” variant,<sup>29</sup> where  $\phi$  is incremented by a constant  $\Delta\phi$  at each resampling. The polarization trajectory between resamplings of straight ECMC is a straight line. In the periodic variant, subsequent straight-line trajectories are at right angles. They are at an angle  $\Delta\phi$  in the sequential variant (see Fig. 2a for an example in  $N = 1$ ). The described variants have very different time evolutions. The polarization trajectories of the sequential variant, for example, persistently rotate for  $N = 1$ , with a total rotation angle that diverges as  $\Delta\phi$  goes to zero.<sup>29</sup>

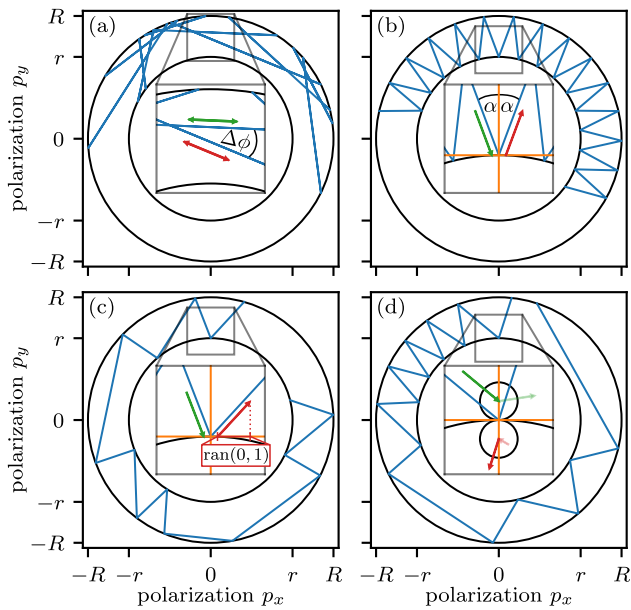


FIG. 2. Sample trajectories for a single tethered dipole. The polarization  $\mathbf{p}$  is the oriented vector between the two disk centers. (a): Sequential variant of straight ECMC.<sup>29</sup> (b): Reflective ECMC.<sup>11</sup> (c): Forward ECMC.<sup>30</sup> (d): Newtonian ECMC.<sup>31</sup>

At a resampling of straight ECMC at time  $t_{\text{res}}$  (usually a multiple of  $\tau_{\text{chain}}$ ), the angle  $\phi$  is updated, but the active disk must also be chosen randomly in order to satisfy global balance. To motivate this, we show for  $N = 1$  that the two disks 1 and 2 must be active with the same probability at time  $t_{\text{res}}$ . Up until the next resampling, all polarizations  $\mathbf{p}(t)$  lie on a segment of the ring  $\Omega$ , and each of the two directions of motion on that segment corresponds to one of the two disks being active (see Fig. 3a). Global balance requires the flows into  $\mathbf{p}(t)$  to be independent of its position. It can be reached from two polarizations  $\mathbf{p}(t_{\text{res}})$  and  $\mathbf{p}'(t_{\text{res}})$ . Depending on the value of  $\mathbf{p}(t)$ , the corresponding polarizations  $\mathbf{p}(t_{\text{res}})$  and  $\mathbf{p}'(t_{\text{res}})$  either both correspond to disk 1 being active at  $t_{\text{res}}$ , or both to disk 2, or one to 1 and one to 2 (see Fig. 3a). Disks 1 and 2 must thus be equally likely ( $p_1 = p_2$ ) to be active right after the resampling, a “random”-mode condition that is precisely implemented by the resampling of the active disk at  $t_{\text{res}}$ .

To illustrate the relevance of the random-mode requirement, we test for  $N = 1$  the case when the active disk is maintained at a resampling while the angle  $\phi$  is incremented in the sequential variant of straight ECMC (“snake” mode). Clearly, snake mode is incorrect, as it samples  $\Omega$  non-uniformly ( $p_1 \neq p_2$ , see Fig. 3b). It seems to be incorrect even when both disks happen to be initially active with practically the same probability ( $p_1 = p_2$ , see Fig. 3c). In both cases, the snake-mode trajectory is repetitive, and lack of irreducibility in the lifted sample space  $\Omega \times \{\phi\}$  induces a non-uniform distribution in  $\Omega$ . For  $N > 1$  at very low density, sequential

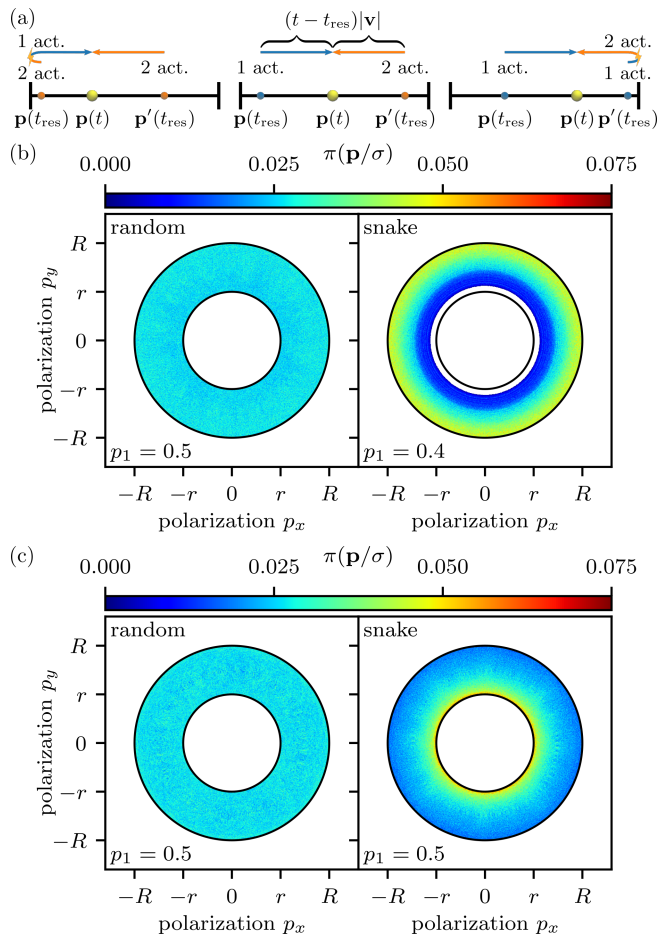


FIG. 3. Global balance and irreducibility for sequential ECMC. (a): Flow into polarization  $\mathbf{p}(t)$  from  $\mathbf{p}(t_{\text{res}})$  and  $\mathbf{p}'(t_{\text{res}})$  on a segment of  $\Omega$  as in Fig. 2a. Events take place at the boundaries of the segment, and the active disk changes. (b): Single-dipole distribution  $\pi(\mathbf{p}/\sigma)$  for sequential ECMC with small  $\Delta\phi$ . The snake-mode distribution is incorrect, and the probability  $p_1$  that disk 1 is active right after a resampling is smaller than  $p_2$ . (c): Same as (b) but for different initial configuration and chain time. The snake-mode distribution is incorrect although both disks are equally likely to be active after a resampling ( $p_1 = p_2$ ).

ECMC in snake mode might not be irreducible, because a single dipole deterministically rotates on a closed trajectory. However, no difference between snake mode and random mode is detected for  $N > 1$  at the higher densities considered in Section IV.

### C. Reflective ECMC

Reflective ECMC<sup>11</sup> differs from the straight ECMC only in its handling of events. At an event, the velocity of the incoming active disk is reflected by the line connecting the active and the target disks, and it becomes the velocity of the target disk. The absolute value of the velocity is thus preserved. For  $N = 1$ , the polarization

follows straight lines which are symmetrically reflected off the inner and outer ring boundaries, with a single reflection angle  $\alpha$  (see Fig. 2b).

Reflective ECMC satisfies global balance for any number of dipoles. For  $N = 1$ , and for an initial velocity that is nearly perpendicular to the separation between the two disks, the polarization may follow a “whispering-gallery-mode” trajectory which never visits small separations  $\rho \gtrsim r$  (compare with Ref. 23, Fig. 3), showing that resamplings of the active disk and of its velocity angle are required for irreducibility. For all initial velocities at  $N = 1$ , even for those that visit all of sample space  $\Omega$ , the probability distribution in the lifted sample space does not separate into independent distributions, and the sampled stationary distribution in  $\Omega$  is non-uniform, and thus incorrect. With periodic resamplings, the stationary distribution is uniform in  $\Omega$ . For  $N > 1$  dipoles, in a large enough box, reflective ECMC fails to be irreducible without resamplings, as the dynamics is then deterministic and a single dipole may effectively rotate in a stationary closed trajectory. Nevertheless, at high enough density, we have not observed any difference in static observables with or without resamplings. It thus appears safe to omit them in practical simulations. As we will see in Section IV, resamplings do not improve the decorrelation. Without resamplings, reflective ECMC is free of intrinsic parameters, and somewhat easier to set up. Computational overhead is avoided.

In previous work on hard disks<sup>11</sup> (rather than hard-disk dipoles), reflective ECMC was benchmarked against straight ECMC and found to be considerably slower. In contrast, in the dipole model studied here, reflective ECMC will prove more powerful than straight ECMC, even when the latter runs with optimized intrinsic parameters.

#### D. Forward ECMC

Forward ECMC<sup>30</sup> resembles reflective ECMC in that, after an event, the target-disk velocities of both algorithms are located in the same quadrant of the coordinate system with axes parallel and orthogonal to the line connecting the disks at the event. All velocities are of unit absolute value, but forward ECMC incorporates a random element into each event. More precisely, the component orthogonal to the line connecting the disks at contact is uniformly sampled between 0 and 1 (while reflecting the orthogonal orientation). Its parallel component is determined so that the velocity is of unit norm. For a single dipole, the polarization describes straight lines that are reflected off the inner and outer ring boundaries. However, the outgoing reflection angle is non-deterministic (see Fig. 2c). Forward ECMC is irreducible even for  $N = 1$ , and it requires no resamplings. Also, as we will show in Section IV, resamplings of the velocity and the active disk in intervals of the chain time do not speed up the algorithm.

#### E. Newtonian ECMC

Newtonian ECMC<sup>31</sup> mimics event-driven molecular dynamics.<sup>36</sup> All disks have velocity labels in addition to their positions. The label of the active disk indicates the time derivative of its position, that is, its displacement in time. All other disks are stationary. Events (including those where the maximum dipole separation is reached) take place as in molecular dynamics, with all velocity labels treated on an equal footing, and with equal masses for all disks. The identities of the active and the target disks are interchanged in the event. During the simulation, the absolute value of the active-disk velocity varies. The equilibrium distribution of all velocity labels is uniform on the  $2N$ -dimensional unit sphere, and the root-mean-square velocity  $v_{\text{rms}}$  is conserved. The event rate per unit distance of the Newtonian ECMC equals the one of the other variants, but the event rate per unit time is smaller by  $\sqrt{\pi}/2$ , because of the difference between  $v_{\text{rms}}$  and the mean absolute value for the two-dimensional Gaussian distribution of velocities. All the velocity labels are used as lifting variables. At a resampling, these labels must be sampled from the exact equilibrium distribution (the rescaled Maxwell–Boltzmann distribution for all disks). Without resampling, the choice of the initial velocity labels is arbitrary.

For  $N = 1$ , the polarization trajectory of Newtonian ECMC reflects off the inner and outer ring boundaries but considers both velocity labels at each event (see Fig. 2d). Without resamplings, Newtonian ECMC breaks irreducibility for this single dipole, and it samples an incorrect stationary probability distribution. For  $N \geq 2$ , we find no influence of observable means on the resampling rate, so that the irreducibility problem is probably again due to the high symmetry of the ring geometry in Section 2. In the larger- $N$  dipole systems in Section IV, we furthermore notice that the algorithm becomes faster in the limit of infinite resampling time.

#### IV. AUTOCORRELATIONS FOR $N$ DIPOLES

In the present section, we characterize the local MCMC algorithms of Section III via the autocorrelation dynamics of the polarization. All correlation times  $\tau_{\text{int}}$  refer to averaged integrated autocorrelation times of single components of the polarization. The unit of time corresponds to a single trial move for the Metropolis algorithm or to the mean event time for ECMC. In ECMC, the computational effort is  $\mathcal{O}(1)$  per event, as it is per move in the Metropolis algorithm. For this reason, no effort is made to compare actual CPU times, which would depend on the implementation. Statistical errors are estimated from the difference between autocorrelation times of the  $x$  and  $y$  components of the polarization which, by symmetry, must be the same. For ECMC, we also take into account the uncertainty in the mean event time. Single MCMC-run times, for each parameter set, are at least

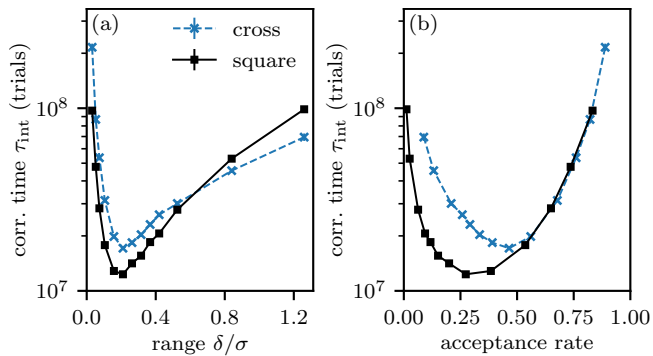


FIG. 4. Correlation time  $\tau_{\text{int}}$  of the Metropolis algorithm with cross- and square-shaped displacement sets for  $N = 81$  dipoles at density  $D = 0.70$ . (a):  $\tau_{\text{int}}$  vs. the range  $\delta$ . (b):  $\tau_{\text{int}}$  vs. acceptance rate. The minimum of  $\tau_{\text{int}}$  provides the reference in Fig. 5, that the ECMC algorithms are benchmarked against.

three orders of magnitude longer than  $\tau_{\text{int}}$ .

### A. Intrinsic parameters of Metropolis and straight ECMC

The correlation time of the local Metropolis algorithm depends on its intrinsic parameters, namely the range  $\delta$  and the displacement set (see Fig. 4a). The acceptance rate decreases with increasing  $\delta$ . The correlation time can thus be expressed as a function of the acceptance rate. As in many comparable models, the “one-half” rule<sup>37</sup> is roughly respected, and the Metropolis algorithm converges best for a rejection rate on the order of 50%. For  $N = 81$  dipoles at density  $D = 0.70$ , we observe a broad optimum between 20% to 40% for the square-shaped displacement set and an optimum close to 50% for the cross-shaped displacement set (see Fig. 4b).

All ECMC variants allow for resamplings so that their correlation times depend on the intrinsic parameter  $\tau_{\text{chain}}$ . The performance of the sequential variant of straight ECMC also depends on the angle increment  $\Delta\phi$ . Without resamplings, straight ECMC is not irreducible and its correlation time is infinite. The optimum  $\tau_{\text{int}}$  is thus at a finite  $\tau_{\text{chain}}$ , to be obtained by fine-tuning (see upper curves in Fig. 5). In its sequential variant, the cases  $\Delta\phi = \pi/2$  and  $\Delta\phi = \pi/3$  make the velocity cycle through a few values only. For these cases, we notice that  $\tau_{\text{int}}$  has two local minima, both of which are rather large. In the absence of a heuristic for the choice of intrinsic parameters, straight ECMC requires explicit fine-tuning, which increases its computational complexity.

As discussed in Section III, reflective, forward and Newtonian ECMC appear irreducible for  $N > 1$  even without resampling and are fastest in this limit  $\tau_{\text{chain}} \rightarrow \infty$  (see lower curves in Fig. 5). This was also observed, e.g., for reflective ECMC in two-dimensional hard-disk systems,<sup>11</sup> and for Newtonian ECMC in three-dimensional hard spheres.<sup>31</sup> For moderate values of

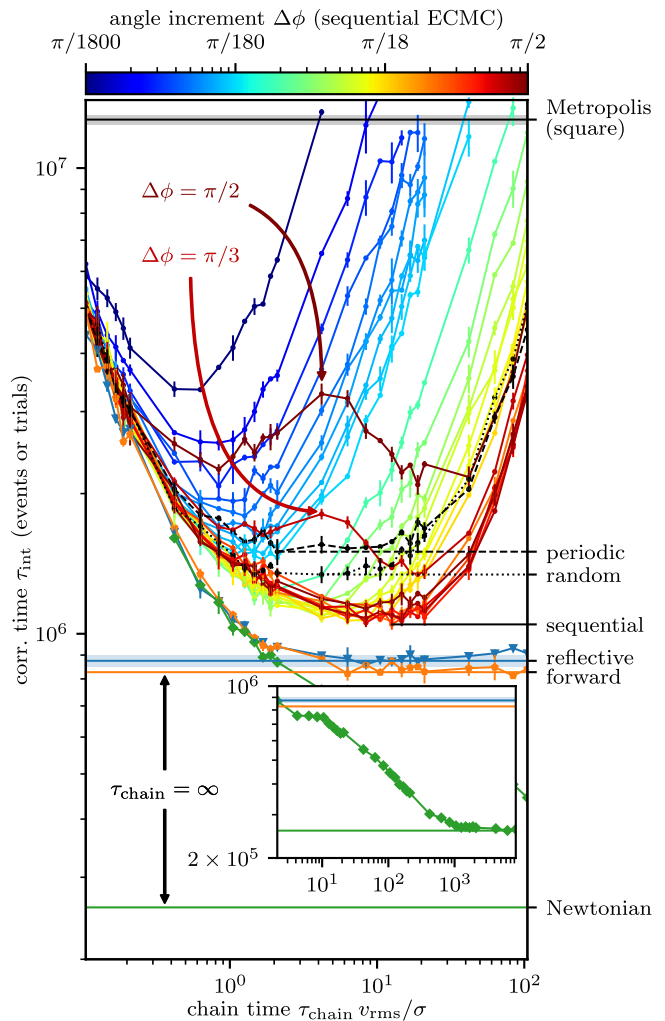


FIG. 5. Correlation times of ECMC variants for different intrinsic parameters (chain time  $\tau_{\text{chain}}$ , angle increment  $\Delta\phi$ ) for  $N = 81$  dipoles at density  $D = 0.70$ . Optimal values of  $\tau_{\text{int}}$  are highlighted on the right y-axis. For reflective, forward, and Newtonian ECMC, they agree with those for  $\tau_{\text{chain}} \rightarrow \infty$ . The optimal performance of the Metropolis algorithm is indicated as the benchmark reference (see Fig. 4). The inset illustrates the evolution of  $\tau_{\text{int}}$  for large  $\tau_{\text{chain}}$  for Newtonian ECMC.

$\tau_{\text{chain}}$ , Newtonian ECMC is comparable to other variants. However, for much larger  $\tau_{\text{chain}}$ , its correlation times again decrease strongly (see inset of Fig. 5). For  $N = 81$  dipoles at density  $D = 0.70$ , the variants that require no fine-tuning perform best. Newtonian ECMC without resampling accelerates with respect to the local Metropolis algorithm by a surprising factor 50 at density 0.70, that seems to further increase at even higher density (see Section IV B).

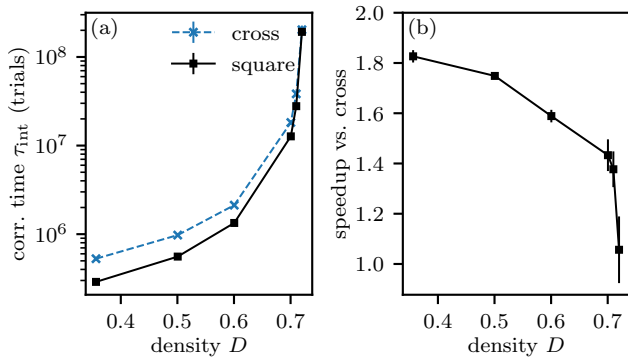


FIG. 6. Performance of the Metropolis algorithm for  $N = 81$  dipoles (optimized intrinsic parameters). (a): Correlation time  $\tau_{\text{int}}$  vs. density  $D$  for the cross- and square-shaped displacement sets. (b): Speedup for the square-shaped displacement set compared to the cross-shaped displacement set.

### B. Density and size dependence of speedups

For both versions of the Metropolis algorithms,  $\tau_{\text{int}}$  naturally increases at higher densities and climbs steeply for  $D \gtrsim 0.70$ , around the liquid–hexatic phase-transition density of the hard-disk system without the tether constraint (see Fig. 6a, again for  $N = 81$ ). For the Metropolis algorithm, the square-shaped displacement set is somewhat preferable over the cross-shaped displacement set for small densities, but the two become equally fast at large densities (see Fig. 6b). This illustrates that, while step-size control is a key feature in reversible MCMC, the details of a local reversible algorithm do not really depend on the displacement sets. For simplicity, we chose the optimal acceptance rates for  $D = 0.70$  for these runs at other densities (see Fig. 4).

For the correlation times of the straight ECMC variants, we perform systematic scans as in Section IV A, for each density at  $N = 81$ . For forward, reflective, and Newtonian ECMC, we use  $\tau_{\text{chain}} = \infty$  without any fine-tuning. For all ECMC variants,  $\tau_{\text{int}}$  increases with density (see Fig. 7a). The periodic variant, which is fastest for two-dimensional hard disks, is the slowest variant for hard-disk dipoles. The random and sequential variants are somewhat faster. Reflective and forward ECMC resemble each other in performance at all  $D$ . While they are considerably faster than the straight variants at low  $D$ , this gap vanishes at  $D = 0.72$ . Newtonian ECMC is the fastest algorithm for all densities and, as mentioned, it requires no fine-tuning. All ECMC algorithms outperform the Metropolis algorithm by a considerable margin (see Fig. 7b). With increasing density, the speedup of reflective and of forward ECMC drops from roughly 30 to 15, while the speedup of the straight ECMC variants increases with density until they become comparable. These trends were similarly observed near the liquid–hexatic transition of two-dimensional hard disks for periodic and reflective ECMC<sup>11</sup> (where the periodic variant, however, was considerably faster than reflective ECMC

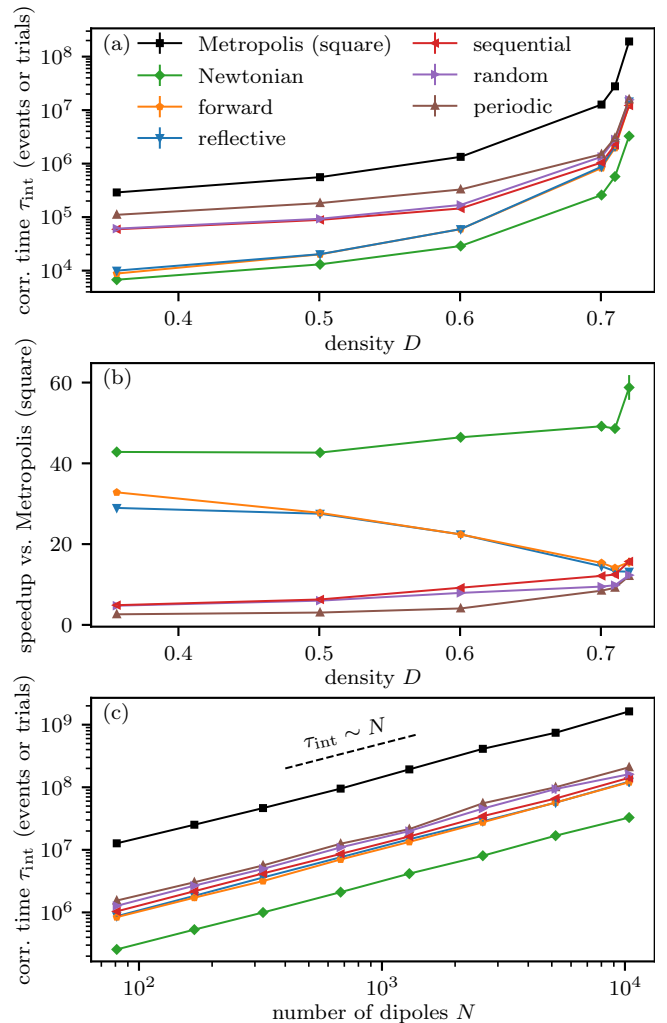


FIG. 7. Performance of ECMC variants and of the Metropolis algorithm with a square-shaped displacement set (where applicable: with optimized intrinsic parameters). (a): Correlation time  $\tau_{\text{int}}$  for  $N = 81$  dipoles vs. density  $D$ . (b): Speedup of ECMC with respect to the Metropolis algorithm. (c): Correlation time  $\tau_{\text{int}}$  at density  $D = 0.70$  vs. number of dipoles  $N$ .

at high densities). The speedup realized by Newtonian ECMC improves slightly from low to high densities, as was likewise found for three-dimensional hard spheres.<sup>31</sup> We observe the highest speedup of roughly a factor of 60 at the highest density  $D = 0.72$  that we studied.

We finally study the dependence of the correlation time  $\tau_{\text{int}}$  of the number of dipoles  $N$  at the density  $D = 0.70$ . For the reflective, forward and Newtonian ECMC variants, we simply set  $\tau_{\text{chain}} = \infty$ , given our findings at  $N = 81$ . For periodic, random and sequential ECMC, we infer the optimal  $\tau_{\text{chain}}$  and  $\Delta\phi$  from the  $N = 81$  case (performing occasional sweeps through intrinsic parameters as cross-checks). For the Metropolis algorithm, we used the optimal acceptance rate of  $N = 81$ . We observe that  $\tau_{\text{int}}$  increases linearly with  $N$  for all algorithms (see

Fig. 7c). This implies that the observed speedups of the non-reversible algorithms stay constant.

## V. CONCLUSIONS AND OUTLOOK

In this paper, we have systematically studied local MCMC algorithms for complex molecules that we caricatured as hard-disk dipoles with parameters inspired by the SPC/Fw water system. Moving from three to two spatial dimensions and from a liquid of charged molecules to a model of hard-disk dipoles has greatly simplified the algorithm development and its implementation. This allowed us to scan thousands of parameters sets for different ECMC variants and to benchmark them against the reversible local Metropolis algorithm. At this exploratory stage, this would have required prohibitive computing resources for the original three-dimensional model.<sup>28</sup> The broad spread of the performance of different ECMC versions came as a surprise. We found that algorithms with intrinsic parameters perform considerably less well than others and demonstrated a 60-fold speedup of Newtonian ECMC with respect to the Metropolis algorithm. Our study has also brought out subtleties of ECMC, that are hidden in simple liquids. For the case of a single dipole, we discovered strict requirements for resampling in order to ensure irreducibility of straight, reflective and Newtonian ECMC. However, these requirements did not seem to play a role for denser systems of dipoles. Event-based randomness as in forward ECMC (or as in all ECMC simulations of soft interactions) strictly ensures irreducibility.

We believe that our observations will carry over from the caricature two-dimensional dipoles to the three-dimensional SPC/Fw systems and related models. There are two reasons why we have not yet studied this system directly. One is, as mentioned, the scale of the computing requirements for a full-fledged three-dimensional scan. The other is that further algorithm development is still required. The cell-veto algorithm<sup>38</sup> (which reduces the computational complexity of the Coulomb problem to  $\mathcal{O}(N \log N)$  per sweep of events, without evaluating the Coulomb energy) is in the present version of our open-source project only implemented for the periodic variant of straight ECMC. However, we expect it to generalize to all ECMC variants for flexible water molecules with an explicit Coulomb interaction. The benchmark against Metropolis MCMC will then be much more favorable, as the change of the Coulomb energy can there only be computed in  $\mathcal{O}(N^{3/2})$  per sweep of moves.<sup>39</sup> The key question will be whether the dynamic arrest of straight ECMC for the three-dimensional water system can be overcome as in the two-dimensional hard-disk dipole model studied here. The extreme dependence of the performance of non-reversible MCMC on details of the algorithm was also evidenced in the escape times from a tightly confined initial configuration,<sup>35</sup> which might be relevant for overcoming dynamic arrest.

Finally, we point out that any tethered-dipole configuration is also a valid hard-disk configuration, with an added upper limit on the distance between pairs of hard disks. For the tethered dipole system, the global hexatic orientational order parameter  $\psi_6$  (see Refs. 14 and 40), at densities  $D \gtrsim 0.70$ , decorrelates faster than for the hard-disk system which there already enters the mixed hexatic–fluid phase. This observed effect might allow for an improved sampling algorithm for hard disks. It is also unclear why straight ECMC performs worse for dipoles than the reflective, forward, and Newtonian variants, while for simple hard disks straight ECMC is clearly the most efficient.

## ACKNOWLEDGMENTS

P. H. acknowledges support from the Studienstiftung des deutschen Volkes and from Institut Philippe Meyer. W. K. acknowledges support from the Alexander von Humboldt Foundation.

## ADDITIONAL REMARKS

The figures in this paper were prepared with the Matplotlib<sup>41</sup> and Visual Molecular Dynamics<sup>42</sup> (VMD) software packages. Integrated autocorrelation times were computed by the Python `emcee` package.<sup>43</sup>

- <sup>1</sup>N. Metropolis, A. W. Rosenbluth, M. N. Rosenbluth, A. H. Teller, and E. Teller, “Equation of State Calculations by Fast Computing Machines,” *J. Chem. Phys.* **21**, 1087–1092 (1953).
- <sup>2</sup>D. A. Levin, Y. Peres, and E. L. Wilmer, *Markov Chains and Mixing Times* (American Mathematical Society, 2008).
- <sup>3</sup>B. A. Berg, *Markov Chain Monte Carlo simulations and their statistical analysis: with web-based Fortran code* (World Scientific, 2004).
- <sup>4</sup>R. Ren, C. J. O’Keeffe, and G. Orkoulas, “Sequential Metropolis Algorithms for Fluid Simulations,” *Int. J. Thermophys.* **28**, 520–535 (2007).
- <sup>5</sup>R. J. Glauber, “Time-Dependent Statistics of the Ising Model,” *J. Math. Phys.* **4**, 294–307 (1963).
- <sup>6</sup>M. Creutz, “Monte Carlo study of quantized SU(2) gauge theory,” *Phys. Rev. D* **21**, 2308–2315 (1980).
- <sup>7</sup>S. Geman and D. Geman, “Stochastic Relaxation, Gibbs Distributions, and the Bayesian Restoration of Images,” *IEEE Trans. Pattern Anal. Mach. Intell.* **PAMI-6**, 721–741 (1984).
- <sup>8</sup>P. Diaconis, S. Holmes, and R. M. Neal, “Analysis of a nonreversible Markov chain sampler,” *Ann. Appl. Probab.* **10**, 726–752 (2000).
- <sup>9</sup>F. Chen, L. Lovász, and I. Pak, “Lifting Markov Chains to Speed up Mixing,” *Proceedings of the 17th Annual ACM Symposium on Theory of Computing*, 275 (1999).
- <sup>10</sup>K. S. Turitsyn, M. Chertkov, and M. Vucelja, “Irreversible Monte Carlo algorithms for efficient sampling,” *Physica D* **240**, 410–414 (2011).
- <sup>11</sup>E. P. Bernard, W. Krauth, and D. B. Wilson, “Event-chain Monte Carlo algorithms for hard-sphere systems,” *Phys. Rev. E* **80**, 056704 (2009).
- <sup>12</sup>M. Michel, S. C. Kapfer, and W. Krauth, “Generalized event-chain Monte Carlo: Constructing rejection-free global-balance algorithms from infinitesimal steps,” *J. Chem. Phys.* **140**, 054116 (2014).



- <sup>13</sup>W. Krauth, “Event-Chain Monte Carlo: Foundations, Applications, and Prospects,” *Front. Phys.* **9**, 229 (2021).
- <sup>14</sup>E. P. Bernard and W. Krauth, “Two-Step Melting in Two Dimensions: First-Order Liquid-Hexatic Transition,” *Phys. Rev. Lett.* **107**, 155704 (2011).
- <sup>15</sup>M. Michel, J. Mayer, and W. Krauth, “Event-chain Monte Carlo for classical continuous spin models,” *EPL* **112**, 20003 (2015).
- <sup>16</sup>Y. Nishikawa, M. Michel, W. Krauth, and K. Hukushima, “Event-chain algorithm for the Heisenberg model: Evidence for  $z \simeq 1$  dynamic scaling,” *Phys. Rev. E* **92**, 063306 (2015).
- <sup>17</sup>K. Kimura and S. Higuchi, “Anomalous diffusion analysis of the lifting events in the event-chain Monte Carlo for the classical XY models,” *EPL* **120**, 30003 (2017).
- <sup>18</sup>D. Müller, T. A. Kampmann, and J. Kierfeld, “Chaining of hard disks in nematic needles: particle-based simulation of colloidal interactions in liquid crystals,” *Sci. Rep.* **10**, 12718 (2020).
- <sup>19</sup>T. A. Kampmann, D. Müller, L. P. Weise, C. F. Vorsmann, and J. Kierfeld, “Event-Chain Monte-Carlo Simulations of Dense Soft Matter Systems,” *Front. Phys.* **9**, 96 (2021).
- <sup>20</sup>M. Hasenbusch and S. Schaefer, “Testing the event-chain algorithm in asymptotically free models,” *Phys. Rev. D* **98**, 054502 (2018).
- <sup>21</sup>M. H. A. Davis, “Piecewise-Deterministic Markov Processes: A General Class of Non-Diffusion Stochastic Models,” *J. R. Stat. Soc. Series B Stat. Methodol.* **46**, 353–376 (1984).
- <sup>22</sup>J. Bierkens, P. Fearnhead, and G. Roberts, “The Zig-Zag process and super-efficient sampling for Bayesian analysis of big data,” *Ann. Stat.* **47**, 1288–1320 (2019).
- <sup>23</sup>A. Bouchard-Côté, S. J. Vollmer, and A. Doucet, “The Bouncy Particle Sampler: A Nonreversible Rejection-Free Markov Chain Monte Carlo Method,” *J. Am. Stat. Assoc.* **113**, 855–867 (2018).
- <sup>24</sup>Z. Lei and W. Krauth, “Mixing and perfect sampling in one-dimensional particle systems,” *EPL* **124**, 20003 (2018).
- <sup>25</sup>M. F. Faulkner, L. Qin, A. C. Maggs, and W. Krauth, “All-atom computations with irreversible Markov chains,” *J. Chem. Phys.* **149**, 064113 (2018).
- <sup>26</sup>P. Höllmer, L. Qin, M. F. Faulkner, A. Maggs, and W. Krauth, “JeLLyFysh-Version1.0 — a Python application for all-atom event-chain Monte Carlo,” *Comput. Phys. Commun.* **253**, 107168 (2020).
- <sup>27</sup>Y. Wu, H. L. Tepper, and G. A. Voth, “Flexible simple point-charge water model with improved liquid-state properties,” *J. Chem. Phys.* **124**, 024503 (2006).
- <sup>28</sup>L. Qin, *Application of irreversible Monte Carlo in realistic long-range systems*, Phd thesis, Université Paris Sciences et Lettres (2020).
- <sup>29</sup>L. Qin, P. Höllmer, and W. Krauth, “Fast sequential Markov chains,” (2020), arXiv:2007.15615 [cond-mat.stat-mech].
- <sup>30</sup>M. Michel, A. Durmus, and S. Sénécal, “Forward Event-Chain Monte Carlo: Fast Sampling by Randomness Control in Irreversible Markov Chains,” *J. Comput. Graph. Stat.* **29**, 689–702 (2020).
- <sup>31</sup>M. Klement and M. Engel, “Efficient equilibration of hard spheres with Newtonian event chains,” *J. Chem. Phys.* **150**, 174108 (2019).
- <sup>32</sup>C. Dress and W. Krauth, “Cluster algorithm for hard spheres and related systems,” *J. Phys. A: Math. Gen.* **28**, L597–L601 (1995).
- <sup>33</sup>J. Liu and E. Luijten, “Rejection-Free Geometric Cluster Algorithm for Complex Fluids,” *Phys. Rev. Lett.* **92**, 035504 (2004).
- <sup>34</sup>K. Börözy, “Über stabile Kreis- und Kugelsysteme,” *Ann. Univ. Sci. Budapest. Eötvös Sect. Math.* **7**, 79–82 (1964).
- <sup>35</sup>P. Höllmer, N. Noirault, B. Li, A. C. Maggs, and W. Krauth, “Sparse hard-disk packings and local markov chains,” (2021), arXiv:2109.13343 [cond-mat.stat-mech].
- <sup>36</sup>B. J. Alder and T. E. Wainwright, “Phase Transition for a Hard Sphere System,” *J. Chem. Phys.* **27**, 1208–1209 (1957).
- <sup>37</sup>W. Krauth, *Statistical Mechanics: Algorithms and Computations* (Oxford University Press, 2006).
- <sup>38</sup>S. C. Kapfer and W. Krauth, “Cell-veto Monte Carlo algorithm for long-range systems,” *Phys. Rev. E* **94**, 031302 (2016).
- <sup>39</sup>H. Berthoumieux and A. C. Maggs, “Collective dispersion forces in the fluid state,” *EPL* **91**, 56006 (2010).
- <sup>40</sup>D. R. Nelson and B. I. Halperin, “Dislocation-mediated melting in two dimensions,” *Phys. Rev. B* **19**, 2457–2484 (1979).
- <sup>41</sup>J. D. Hunter, “Matplotlib: A 2d graphics environment,” *Comput. Sci. Eng.* **9**, 90–95 (2007).
- <sup>42</sup>W. Humphrey, A. Dalke, and K. Schulten, “VMD – Visual Molecular Dynamics,” *J. Mol. Graph.* **14**, 33–38 (1996).
- <sup>43</sup>D. Foreman-Mackey, D. W. Hogg, D. Lang, and J. Goodman, “emcee: The MCMC Hammer,” *Publ. Astron. Soc. Pac.* **125**, 306 (2013).